Centrin: Its Secondary Structure in the Presence and Absence of Cations†

Belinda Pastrana-Rios,*,‡ Wanda Ocaña,‡ Michelle Rios,‡ German Lorenzo Vargas,‡ Ginny Ysa,‡ Gregory Poynter,§ Javier Tapia,‡ and Jeffrey L. Salisbury§

Department of Chemistry, University of Puerto Rico Mayagüez Campus, Mayagüez, Puerto Rico 00681-9019, and Department of Biochemistry and Molecular Biology, Mayo Clinic and Foundation, Rochester, Minnesota 55095

Received September 25, 2001; Revised Manuscript Received April 5, 2002

ABSTRACT: Centrin is a low molecular mass (20 kDa) protein that belongs to the EF-hand superfamily of calcium-binding proteins. Local and overall changes were investigated for interactions between cations and *Chlamydomonas* centrin using Fourier transform infrared (FT-IR) and circular dichroic (CD) spectroscopies. FT-IR spectral features studied included the amide I′ band and the side-chain absorbances for aspartate residues located almost exclusively at the calcium-binding sites in the spectral region of 1700−1500 cm^{-1}. The amide I′ band is exquisitely sensitive to changes in protein secondary structure and is observed to shift from 1626.5 to 1642.7 cm^{-1} in the presence and absence of calcium. These spectral bands are complex and were further studied using two-dimensional Fourier transform infrared (2D-FT-IR) correlation along with curve-fitting routines. Using these methods the secondary structure contributions were determined for holocentrin and apocentrin. The α-helical content in centrin was determined to be 60%−53% in the presence and absence of cations, respectively. Furthermore, the *β*-strand content was determined to be 12%−36%, while the random coil component remained almost constant at 7%−13.5% in the presence and absence of cations, respectively. Changes in the side-chain band are mostly due to the monodentate coordination of aspartate to the cation. A shift of ∼4 cm^{-1} (for the COO^- antisymmetric stretch in Asp) from 1565 to 1569 cm^{-1} is observed for apocentrin and holocentrin, respectively. Thermal dependence revealed reversible conformational transition temperatures for apocentrin at 37 °C and holocentrin at 45 °C, suggesting greater stability for holocentrin.

Centrin is an acidic, low molecular weight (M_r ∼20000) protein that belongs to the EF-hand superfamily of calcium-binding proteins (*1*, *2*). This calcium-binding protein (centrin) was first identified as a major component of the fibers that link the nucleus to the flagellar apparatus in flagellated unicells (*3*, *4*), and later, it was shown to be a ubiquitous component of centrioles, centrosomes, and mitotic spindle poles (*5*). A distinguishing feature of centrin-based fiber systems is that they all show calcium-induced contractile behavior, which typically results in a dramatic and rapid change in the orientation of centrioles relative to one another and to the nucleus or to changes in the overall shape and extent of the centrosome (*3*, *6*, *7*).

Little is known about the molecular basis for centrin-based fiber contraction or about the association of accessory proteins in centrin-based fibers. Furthermore, the precise role of calcium binding in the contraction process remains unclear (*8*). Conflicting results have been reported using circular dichroic (CD)[1] analyses to demonstrate the effects of calcium on protein conformation. Huang and co-workers (*9*) reported no significant changes in the CD spectrum, while Wiech and co-workers (*10*) reported an overall increase in the α-helical content of the molecule upon calcium binding. We, therefore, have undertaken a careful examination of the biophysical properties of centrin. These studies utilize highly purified preparations of bacterially expressed recombinant centrin. This material was subjected to Fourier transformed infrared (FT-IR) and CD spectroscopies to assess the effects of calcium binding on protein secondary structure. The amide I′ band is very sensitive to backbone conformation and is representative of several structural domains (*11*, *12*). Two-dimensional Fourier transform infrared (2D-FT-IR) correlation (*13*) along with curve fitting were used to analyze the spectral data. This novel approach toward the study of protein or peptide conformational changes and specific side-chain interactions has proven to be useful (*14*, *15*). We have used this combined FT-IR, two-dimensional correlation analysis and curve-fiiting approach to resolve the conflict in results reported earlier (*9*, *10*). Circular dichroism is a conventional technique for the study of protein conformation (*16*, *17*). In this study, CD was used to confirm the results obtained by FT-IR.

† Research supported by NIH Grant CA72836 (J.L.S.), NRSA Training Grant HDO7108, NSF-EPSCoR and NIH-SCORE Grant 5-S06GM08103 (B.P.-R.), NIH Grant CA 72836 (J.L.S.), the University of Puerto Rico, and the Mayo Clinic and Foundation.

* To whom correspondence should be addressed. E-mail: be_pastrana@rumac.uprm.edu or belinda@hpcf.upr.edu.

‡ University of Puerto Rico.

§ Mayo Clinic and Foundation.

[1] Abbreviations: FT-IR, Fourier transform infrared; CD, circular dichroism; 2D-FT-IR, two-dimensional Fourier transform infrared; D_2O, deuterium oxide; *E. coli*, *Escherichia coli*; IPTG, isopropyl *β*-D-thiogalatopyranoside; SDS−PAGE, sodium dodecyl sulfate−polyacrylamide gel electrophoresis; TOF, time of flight mass spectrometry; EDTA, ethylenediaminetetraacetic acid tetrasodium salt; EGTA, ethylene glycol bis(*β*-aminoethyl ether)-*N*,*N*,*N*′,*N*′-tetraacetic acid; DTT, 1,4-dithiothreitol.

10.1021/bi0157971 CCC: $22.00
Published on Web 05/09/2002

Scheme 1: Schematic Representation Summarizing the Purification Protocol Used for *Chlamydomonas* Centrin

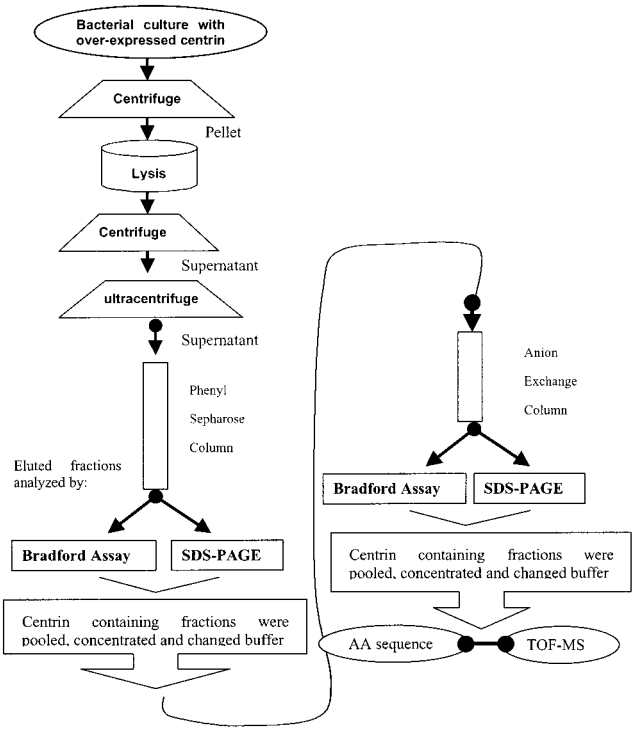

EXPERIMENTAL PROCEDURES

Materials

The materials used were all of the highest purity commercially available and were used without further purification. Deionized H_2O (18 MΩ) and D_2O (99.9% atom D) (Cambridge Isotope Laboratories, Inc., Andover, MA) were used as indicated below. Hepes buffer (Sigma Chemical Co., St. Louis, MO) adjusted to a pH of 7.4 was used for the spectroscopic studies.

Methods

Bacterial Expression and Purification of Centrin. Chlamydomonas centrin was overexpressed off a pt7-5 plasmid construct in *Escherichia coli* BL21 λDE_3 induced with IPTG (Gibco BRL, Ann Habor, MI) to yield milligram quantities of the desired protein. Transformation and expression were done with modifications to the protocol of Baron (*18*). Briefly, transformed *E. coli* cells were grown in 2XYT media (Biol 101, Vista, CA) containing 50 μg/mL ampicillin and incubated at 37 °C while monitoring its growth via OD measurements at 500 nm. Once the cells entered log phase, 0.5 mM IPTG was added to the culture, and 2 h later, the cells were harvested and frozen. The isolation protocol used is summarized in Scheme 1. Frozen cells were thawed in lysis buffer containing a cocktail of protease inhibitors and sonicated with a macro probe (Heat Systems-Ultrasonics Inc., Farmingdale, NY) at maximum power for three 30 s pulses and 1 min rest periods while on ice. The lysate was cream colored and free flowing (low viscosity). This solution was centrifuged at 10000*g* for 15 min at 4 °C. The supernatant was recovered and adjusted to 2 mM $CaCl_2$ and 4 mM $MgCl_2$ followed by a second centrifugation at 100000*g* for 30 min at 4 °C. This solution was filtered using a low protein affinity

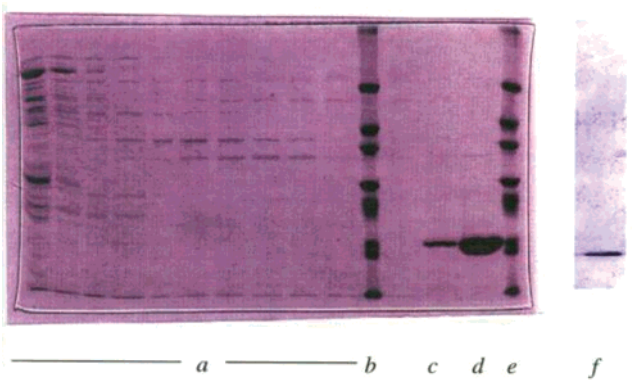

FIGURE 1: 16% bisacrylamide SDS−PAGE developed with Coomassie blue stain. Lanes marked as a are void volume fractions. Lanes b and e are low molecular weight standards (66000, 45000, 36000, 29000 24000, 20000, 14200), and in lanes c and d are fractions containing centrin. Lanes not labeled are eluted fractions prior to the desired buffer for the elution of centrin.

PES membrane filter (Millipore Corp., Bedford, MA) with 2 μm pore size. The filtered supernatant was applied to a phenyl-Sepharose CL-4B (Pharmacia Inc., Piscataway, NJ) column equilibrated with buffer and then eluted with a low-calcium-containing buffer. Fractions containing centrin were identified via SDS−PAGE (Figure 1).

Figure 1 fractions obtained using EGTA and EDTA containing elution buffer were analyzed for protein content and run on an SDS−PAGE. A single intense band with a relative mobility of approximately M_r 20000 was determined to be centrin on the basis of western blot analysis (results not shown). The fractions containing centrin were pooled, concentrated, re-equilibrated in buffer (20 mM Hepes, 1 mM $CaCl_2$, and 1 mM DTT at pH 7.4), and subjected to chromatography using a strong anion-exchange (High Q) column (Bio-Rad, Hercules, CA). Elution using a NaCl gradient was monitored at 280 nm, fractions were collected, and aliquots from every other fraction were analyzed by SDS−PAGE. Fractions containing centrin were pooled for mass spectral analysis and amino acid sequencing. Time of flight (TOF) mass spectrometry was carried out (at the Mayo Mass Spectrometry Core Facility) to determine the molecular mass and purity of centrin. Typical mass spectral results are presented in Figure 2.

Four TOF peaks were observed (Figure 2) with mass/charge ratios of 19255, 9637, 6427, and 4814 for the single, double, triple, and quadruple protonated species, respectively. These results are consistent with the known molecular mass of centrin based on its sequence and demonstrate the relative purity of the preparation to be greater than 99%. To verify its identity, the protein was subjected to an amino-terminal sequence analysis at the Mayo Peptide Core Facility. The sequence results confirm the identity as *Chlamydomonas* centrin and are presented in Table 1.

A portion of the purified recombinant protein was dialyzed extensively at 4 °C using 50 mM Hepes, 150 mM NaCl, 4 mM EDTA, and 4 mM EGTA at pH 7.4 to generate apocentrin. The rest of the sample (holocentrin) was dialyzed against 50 mM Hepes, 150 mM NaCl, 4 mM $CaCl_2$, and 4 mM $MgCl_2$ at pH 7.4.

Centrin's concentration was determined by several methods: colorimetric, nitrogen determination, and direct UV absorbance at 274 nm. The molar extinction coefficient for

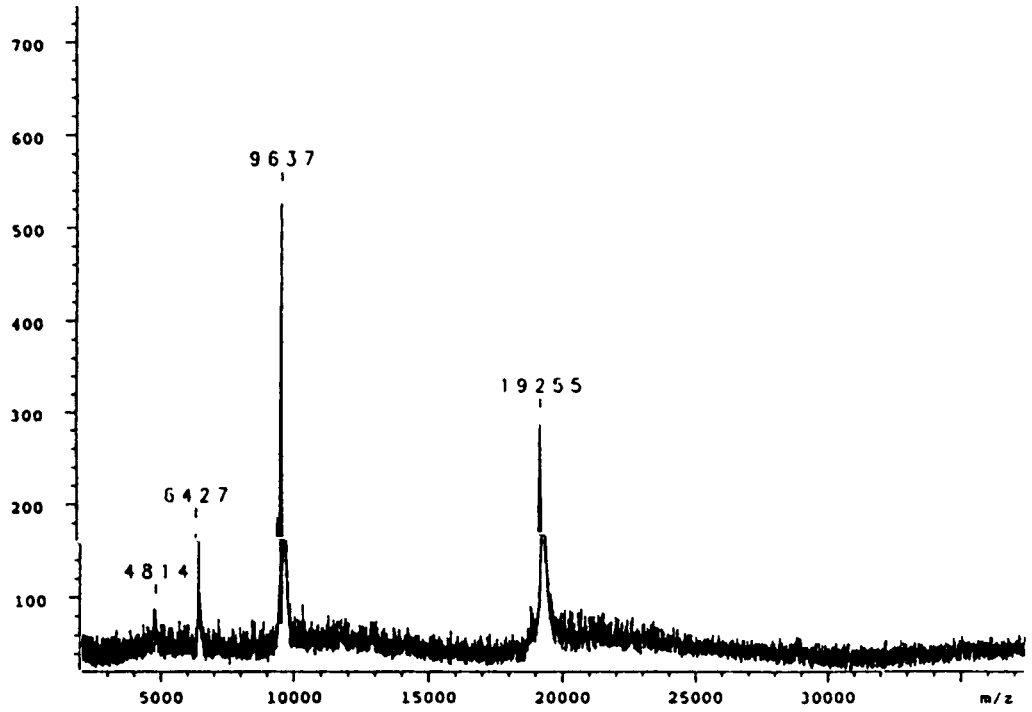

FIGURE 2: TOF mass spectral results demonstrating its high purity by the mass/charge ratios observed. Four TOF peaks with mass/charge ratios of 19255, 9637, 6427, and 4814 for the single, double, triple, and quadruple protonated species are observed. This mass/charge ratio confirms the *Chlamydomonas* centrin molecular weight and demonstrates its relative purity to be >99%.

Table 1: Summary of Amino Acid Sequence Results

cycle no.[a]	1	2	3	4	5	6	7	8	9	10	11	12
amino-terminal analysis	S	Y	K	A	K	T	V	V	S	A	R	R
Chlamydomonas centrin sequence	S	Y	K	A	K	T	V	V	S	A	R	R

[a] This sequence was obtained from signals greater than 100 pmol, and all calls were confident.

this protein was determined to be 1309.9 ± 80.4 and 1136.3 ± 127.6 M^{-1} cm^{-1} in the presence and absence of cations, respectively.

Circular Dichroism. Centrin (2.3 μM) in 8 mM Hepes, 2 mM $CaCl_2$, 2 mM $MgCl_2$, and 50 mM NaCl at pH 7.4 was used for holocentrin, while 13.5 μM apocentrin in 8 mM Hepes, 1 mM EDTA, 1 mM EGTA and 50 mM NaCl at pH 7.4 was used. CD measurements were made on a Jasco J-710 spectropolarimeter (Tokyo, Japan). The instrument was calibrated using (+)-10-camphorsulfonic acid. Five scans, within the spectral range of 250−190 nm, were collected at a scan rate of 20 nm/min to yield each spectrum at the desired equilibrated temperature. Temperature dependence spectra were also collected from 0 to 85 °C while monitoring at 222 nm.

FT-IR Spectroscopy. Spectra were collected following complete H → D exchange in the centrin preparation. For this, the protein was dialyzed under the desired conditions and then lyophilized repeatedly while redissolving the sample in D_2O. A 25 μL aliquot of 24 mg/mL centrin in 50 mM Hepes buffer at pD 6.65 containing 4 mM EGTA, 4 mM EDTA, and 150 mM NaCl in D_2O (for apocentrin) was deposited on a $AgCl_2$ window (Spectral Systems, Hopewell Junction, NJ), and a spacer of 40 μm was set between this and a second window. For holocentrin, 50 mM Hepes buffer containing 4 mM $CaCl_2$, 4 mM $MgCl_2$, and 150 mM NaCl at pD 6.65 in D_2O was used. The complex was deposited in a similar manner as mentioned above using 25 mm CaF_2 windows with a 40 μm spacer. A reference cell was prepared similarly. The temperature within the cell was controlled *via* a Neslab circulating bath (Newington, NH) and monitored with a thermocouple positioned in close contact with the sample. The temperature accuracy was estimated to be within 1 °C. Routinely, 10 min was allowed for thermal equilibrium to be reached before spectral acquisition was begun. The instrument was an FTS-40 Bio-Rad (Cambridge, MA) with custom sample shuttle and interface. Typically, 512 scans were coadded, apodized with a triangular function, and Fourier transformed to provide a resolution of 4 cm^{-1} with the data encoded every 2 cm^{-1}. Eight spectra were collected at sequential increments of temperature, allowing for equilibrium, and used in the two-dimensional FT-IR correlation analysis.

Two-dimensional FT-IR correlation analysis was performed using MathCad 6 (MathSoft, Inc., Cambridge, MA) software. The curve-fitting routines were done using the Grams 3.01 (Galactic Industries Corp., Salem, NH) program. The Origin 6 program was used to plot curve-fitted data.

RESULTS

FT-IR Results. FT-IR spectra were obtained for *Chlamydomonas* centrin as a function of temperature in the presence and absence of cations. The results obtained at 25 °C for holocentrin and apocentrin are shown in Figure 3. There are definite changes in the spectrum due to the coordination of cations, and these changes are not limited to protein conformation. The amide I′ band as well as the side-chain band is shifted by 20 cm^{-1} (1642.7 cm^{-1}, holocentrin; 1626.5 cm^{-1}, apocentrin) and 10 cm^{-1} (1585.7 cm^{-1}, apocentrin;

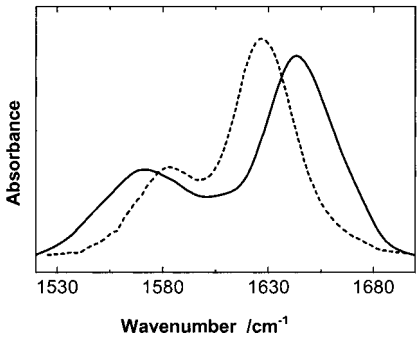

FIGURE 3: Overlaid FT-IR spectra of *Chlamydomonas* centrin: (—) holocentrin and (---) apocentrin in the spectral region of 1720−1510 cm^{-1}.

1576 cm^{-1}, holocentrin), respectively. 2D-FT-IR correlation analysis was used to interpret these results.

2D-FT-IR. FT-IR spectra were studied using two-dimensional correlation techniques developed by Noda et al. (*13*, *20*−*22*). This technique enhances the resolution of the amide I′ band and confirms the curve-fitting analysis. Results obtained for holocentrin are shown in Figure 4. The asynchronous plot (Figure 4B) confirms the existence of the subbands in the synchronous plot (Figure 4A) and therefore was used in the curve-fitting analysis. The results, summarized in Table 2, demonstrate the consistency of the methods for spectral analysis. Subbands of the curve-fitting analysis for the amide I′ band (associated with backbone conformation) were used to simulate the 2D correlation obtained for the experimental spectra (data not shown). The simulated 2D-FT-IR plots (synchronous and asynchronous) were remarkably similar to the experimental plots. In addition, the side-chain bands, mainly due to the vibrational modes, are sensitive to calcium coordination; this is observed by the shift from 1569 to 1565 cm^{-1} for aspartate and 1548 to 1556 cm^{-1} for glutamate in the presence and absence of cations, respectively. This effect on the aspartate band position due to calcium coordination demonstrates the sensitivity of this technique toward the carboxyl dipole.

Table 2: Contributing Bands Obtained from 2D-FT-IR Correlation Analysis for the FT-IR Spectral Region 1720−1500 cm^{-1}

	frequency (cm^{-1})	
sample	synchronous	asynchronous
apocentrin	1657[a]	1668[a]
	1629	1632
	1623	1620
	1599	1600
	1591	1592
	1581	1585
	1557	1561
holocentrin	1658[a]	1664[a]
	1639	1645
	1623	1625
	1592	1592
	1584	1587
	1563	1562
	1557	1555

[a] Assignment for this region is estimated due to the broad nature of the band which can include two overlapped bands that could not be resolved.

Results obtained for apocentrin are shown in panels A and B of Figure 5 for synchronous and asynchronous plots, respectively. The apocentrin two-dimensional plots are markedly different from those obtained for holocentrin, suggesting the possibility of different conformational states.

In the synchronous plots, Figures 4A and 5A for holocentrin and apocentrin, respectively, a series of cross-peaks (peaks observed away from the diagonal) (*20*) are observed. Cross-peaks are generated when two dipole-transition moments (vibrational modes) of different functional groups are reorienting simultaneously. The cross-peaks represent coordinated or cooperative motion of local structures occurring when interactions exist among the functional groups (*20*). These peaks suggest the existence of inter- or intramolecular interactions among the functional groups. More importantly, the synchronous plots in Figure 5A show that the cross-peak due to the aspartate vibration (1565 cm^{-1}) is strongly interacting with the amide I′ band (backbone vibration, 1640

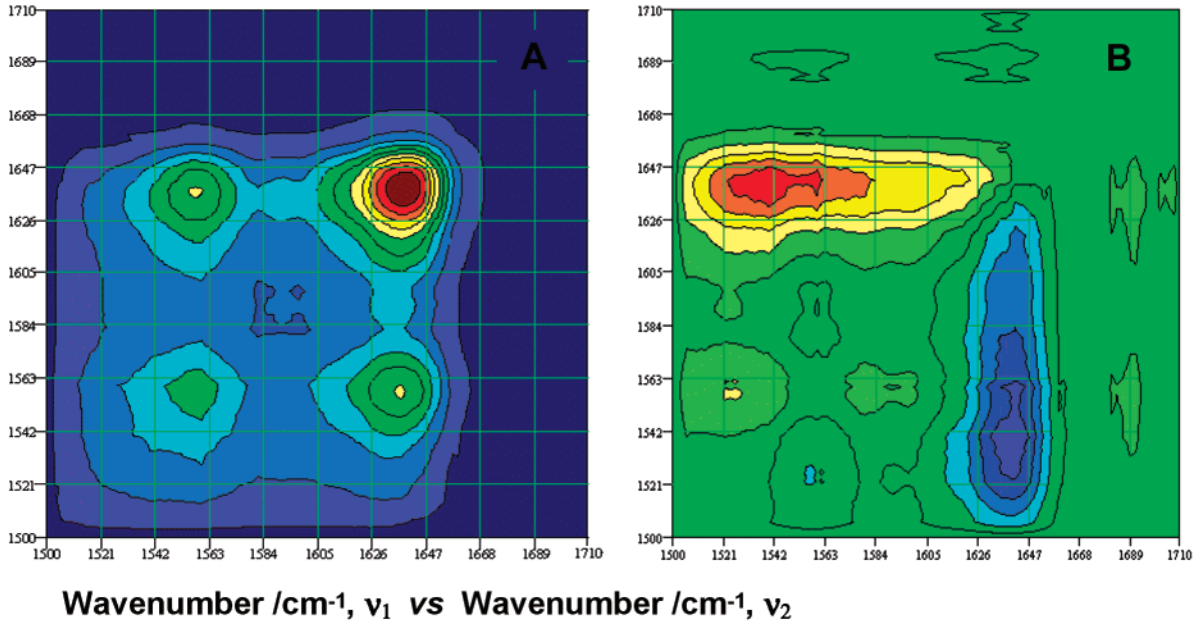

FIGURE 4: 2D-FT-IR contour plots of holocentrin. (A) Synchronous plot and (B) asynchronous plot; colors represent the phase of the peaks.

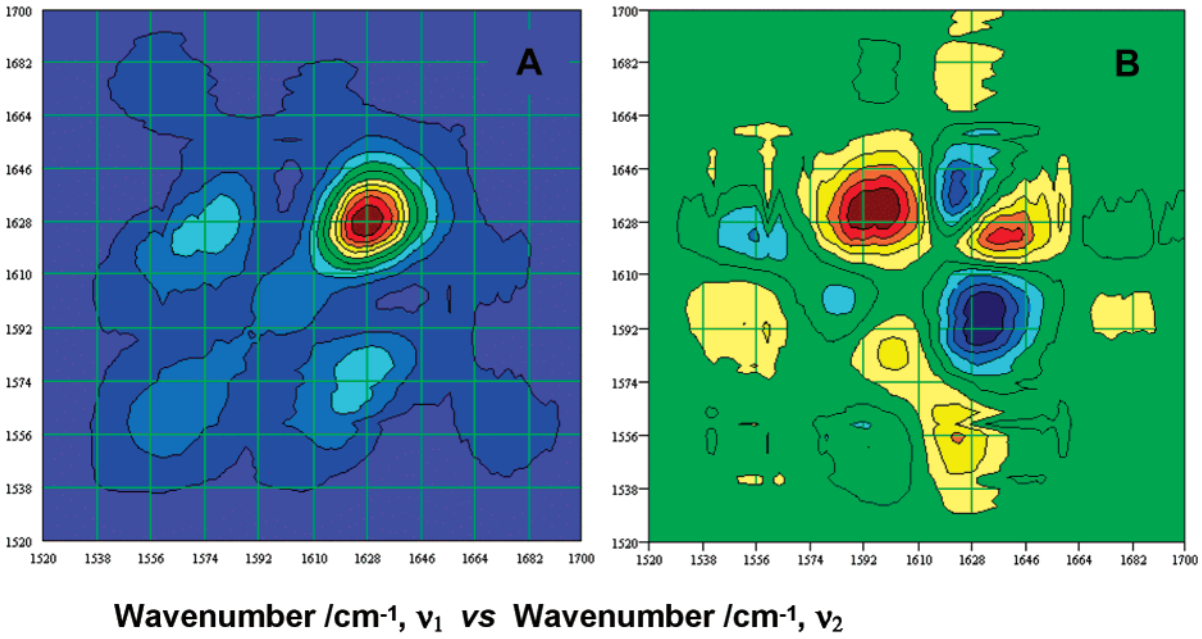

FIGURE 5: 2D-FT-IR contour plots of apocentrin. (A) Synchronous plot and (B) asynchronous plot.

Table 3: Summary of Phase Analysis of the Asynchronous Plots for Apocentrin and Holocentrin

events[a]	apocentrin asynchronous analysis	comment/vibration
1	1628 cm^{-1} occurs prior to 1592 cm^{-1}	β-strand prior to Arg
2	1628 cm^{-1} occurs prior to 1556 cm^{-1}	β-strand prior to Glu^-
3	1570 cm^{-1} occurs prior to 1628 cm^{-1}	Asp^- prior to β-strand
4	1628 cm^{-1} occurs prior to 1660 cm^{-1}	transition from β-strand to random coil

events[a]	holocentrin asynchronous analysis	comment/vibration
1	1631 cm^{-1} occurs prior to 1658 cm^{-1}	β-strand prior to α-helix
2	1631 cm^{-1} occurs prior to 1560 cm^{-1}	β-strand prior to Asp^-
3	1631 cm^{-1} occurs prior to 1587 cm^{-1}	β-strand prior to Arg

[a] Sequence of spectral intensity changes in ascending order of temperature.

cm^{-1}), and in the simulated 2D-FT-IR correlation analysis with only the side-chain modes (data not shown) the aspartate band is correlated to the arginine symmetric and asymmetric stretch bands, thus suggesting coupling between the aspartate and the arginine in the absence of cations. Similar effects have been reported with glutamate and arginine in a model peptide study (*15*).

The asynchronous plots can also describe the time line in which the changes in protein structure occurred. This interpretation is based on the phase of the cross-peaks generated in the asynchronous plots (red is positive and blue is negative). For the apocentrin plot the backbone vibrational mode (1628 cm^{-1}) was affected by thermal perturbation prior to the arginine symmetric stretching vibration (1592 cm^{-1}). These results are summarized in Table 3. The asynchronous plots also verified the existence of the autopeaks (peaks along the diagonal) observed in the synchronous plots, and these peak positions were used to curve-fit the spectra obtained for apocentrin and holocentrin (Table 3).

FT-IR Curve-Fitting Routine. Representative curve-fitting analysis is shown in Figure 6. Subbands associated with the backbone conformation and side-chain absorbances were used to simulate the experimental spectrum. The position

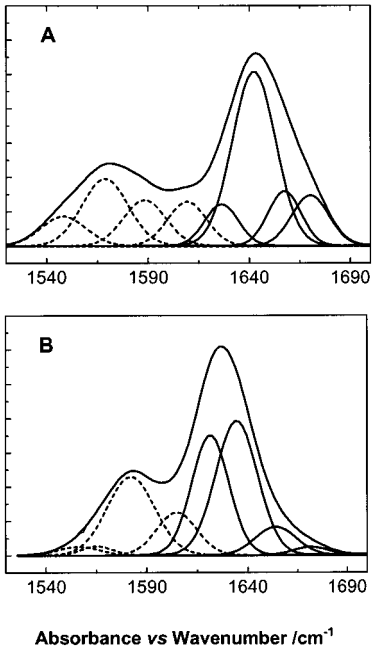

FIGURE 6: Typical curve-fitted FT-IR spectra of *Chlamydomonas* centrin at 25 °C. (—) are the experimental spectrum and (---) are the contributing subbands and simulated spectrum for (A) holocentrin in the spectral region of 1720−1500 cm^{-1} and (B) apocentrin in the spectral region of 1700−1520 cm^{-1}.

and number of subbands used were determined from the 2D-FT-IR correlation analysis presented in Table 2. Furthermore, the subbands used for the curve-fitting analysis in the spectral region of 1520−1700 cm^{-1} at 20 °C in the presence of cations (holocentrin) were at 1642 cm^{-1} (α-helix), 1656 cm^{-1} (loop), 1672 cm^{-1} (random coil), 1625 cm^{-1} (β-strand or aggregation), 1610 and 1587 cm^{-1} (arginine asymmetric and symmetric stretch, respectively), 1568 cm^{-1} (aspartate), and 1548 cm^{-1} (glutamate), while in the absence of cations (apocentrin) the subbands used were at 1622 cm^{-1} (aggregation), 1633 cm^{-1} (β-strand), 1654 cm^{-1} (α-helix), 1672 cm^{-1} (random coil), 1604 and 1581 cm^{-1} (arginine asymmetric and symmetric stretch, respectively), 1566 cm^{-1} (aspartate),

Table 4: Summary of CD Fit Using the Self-Consistent Method (SELCON3) and the FT-IR Curve-Fitting Analysis for Estimating the Secondary Structure below and above the Conformational Transition of Centrin in the Presence and Absence of Cations

spectra	*T*/°C	α-helix/%	β-strand/%	turn/%	random coil/%	sum/%	estd no. of segments for α-helix/β-strand	av no. of residues per segment
					Apocentrin			
CD	5	39.1	3.5	27.6	29.7	99.9	8.3 (α)/1.8 (β)	8 (α)/3.2 (β)
IR	0	53.5	36.4	3.1	7.0	100	n/a[a]	n/a
CD	90	14.3	31.3	21	33.2	99.8	3.5 (α)/9.6 (β)	7 (α)/5.6 (β)
IR	78.4	36	43.6	2.8	17.1	99.5	n/a	n/a
					Holocentrin			
CD	5	60	0.0	16	26.2	102.2	7 (α)/0.5 (β)	15 (α)/0 (β)
IR	3	60	12	14.7	13	99.7	n/a[a]	n/a
CD	90	40.3	14.7	21	25.5	101.5	7 (α)/6.2 (β)	10 (α)/4 (β)
IR	83	53.5	12	20.2	14.2	99.9	n/a	n/a

[a] n/a, not applicable.

and 1556 cm^{-1} (glutamate). Spectral results also render information about holocentrin on side-chain absorbance of aspartate, which is shifted by ~11 cm^{-1} from the model studies carried out by Venyaminov (*26*). Similarly, results were rendered for the glutamate band observed at 1548 cm^{-1} which is shifted by ~12 cm^{-1} when compared to Venyaminov's (*26*) assignments on model side-chain studies. This suggests that the transition dipole moment is affected by coordination with the cation (calcium and/or magnesium). Since, the majority of these residues are found in the cation-binding site, this result gives rise to information about the EF-hand loops in the protein. The aspartate side chains in these loops are involved in coordination with the cation (*23*, *24*, *25*).

Data Analysis. For spectral curve fitting, a series of subband assignments were made for the simulation of the experimental spectra. In the curve-fitting routine the height, position, and width of the subband were not fixed and optimized by least squares minimization. The resulting peak positions could be assigned to a known backbone or frequency summarized in Table 2 for apocentrin and holocentrin. Side-chain vibrational frequencies (*26*, *27*) such as aspartate (1578 cm^{-1}), glutamate (1560 cm^{-1}), and arginine (1586 and 1606 cm^{-1}) were also considered. Resulting band frequencies and assignments are summarized in Table 4 and shown in Figures 6. Overall changes in the protein were also observed by studying the amide I′ band (1630 cm^{-1}). The helical content is estimated to be 60% (3 °C) and 53% (0 °C) in the presence and absence of cations, respectively. The β-strand conformation exposed to its aqueous environment or aggregation constituted 12% (3 °C) and 36.4% (0 °C) for holocentrin and apocentrin, respectively. This β-strand assignment has been reported previously for β-lactoglobulin B (*28*).

Circular Dichroism. CD spectra obtained for *Chlamydomonas* centrin corroborate the results obtained by FT-IR spectroscopy. Greater helical content was observed for holocentrin when compared to apocentrin. The extent of thermal unfolding was studied using CD (Figure 7). Upon first inspection, the spectrum has an isodichroic point, thus suggesting protein conformational changes that do not involve α-helix to random coil transition but rather a different type of transition. Similar results have been obtained for simulated poly-L-lysine CD spectra by Fasmans' group (*29*). In addition, the molar ellipticity [θ] values in deg cm^2 dmol/residue at 222 nm for centrin in the presence of cations were

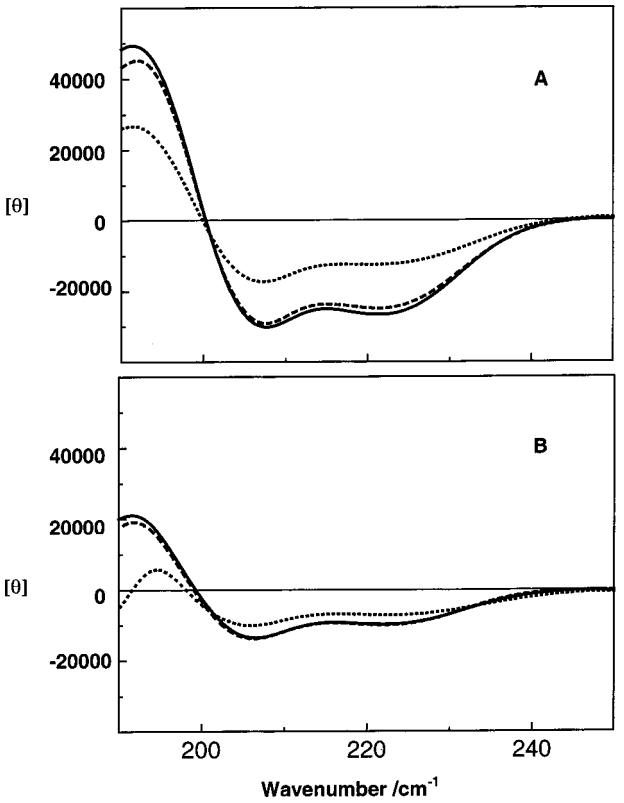

FIGURE 7: Overlaid circular dichroic (CD) spectra of *Chlamydomonas* centrin at (—) 5 °C, (---) 25 °C, and (···) 85 °C in the spectral region of 250−190 nm for (A) holocentrin and (B) apocentrin.

determined to be −25741.3 (5 °C), −24048 (20 °C), and −10621 (90 °C), while in the absence of cations were −11765.7 (5 °C), −11269.9 (20 °C), and −8775.6 (90 °C). These results suggest greater helical content for holocentrin. The spectra were also analyzed by estimating the secondary structural contribution based on following a self-consistent method known as Selcon3 developed Sreerama et al. (*30*−*32*). Matrices of CD spectral data for 29 reference proteins (*33*) were used along with the empirical CD spectrum of centrin under a given condition. The program employs a singular value decomposition algorithm by Forsythe et al. (*34*) and variable selection using the locally linearized model by van Stokkum (*35*). Results obtained for CD spectra acquired at 5 and 90 °C in the presence and absence of cations are summarized in Table 4. The percent helicity of 60% calculated for holocentrin agrees with that from Huang

(*9*) and is consistent with our FT-IR studies in the presence of cations. In addition, the random coil contribution remained relatively constant (~30% for apocentrin and ~26% for holocentrin) with increase in temperature. The analysis of the CD spectra was not limited to the prediction of secondary structure percent contribution, but also the estimation of the number of α-helical and *β*-strand segments and the average length of the segments were determined. These results are also summarized in Table 4. However, upon closer inspection the CD and FT-IR estimates of secondary structure contribution agreed well only in the presence of cations; less agreement (although same tendency) was observed for apocentrin secondary structure estimates that may be due to the spectral data set used in the fitting algorithm.

Thermal Denaturation. Thermal transition was monitored by CD and FT-IR spectroscopies in the range of temperature studied, 0−90 °C, in panels A and B of Figure 8 for centrin in the presence and absence of cations, respectively. The conformational transition temperature (T = 37 °C) for apocentrin was less than the conformational transition temperature (T = 45 °C) observed for holocentrin. This thermal unfolding process was reversible in the presence and absence of cations. Similar transitions have been reported by Cox's group (*40*) using differential scanning calorimetry (DSC) for calcium-binding vector protein (CAVP) which has 30% identity to centrin. In addition, the normalized α-helical fractions as a function of temperature were determined using the area of the α-helical subband determined from the FT-IR curve-fitting analysis. The results summarized in Figure 8C are assuming that the extinction coefficient does not change with temperature. For holocentrin the fraction of α-helical content decreased from 0.60 (0 °C) to 0.46 (83 °C), while for apocentrin the fraction of α-helical content decreased from 0.54 (2.7 °C) to 0.33 (78.4 °C), suggesting a conformational transition. This effect has also been observed in model helical peptides during thermal unfolding (*14*, *15*; manuscript in preparation).

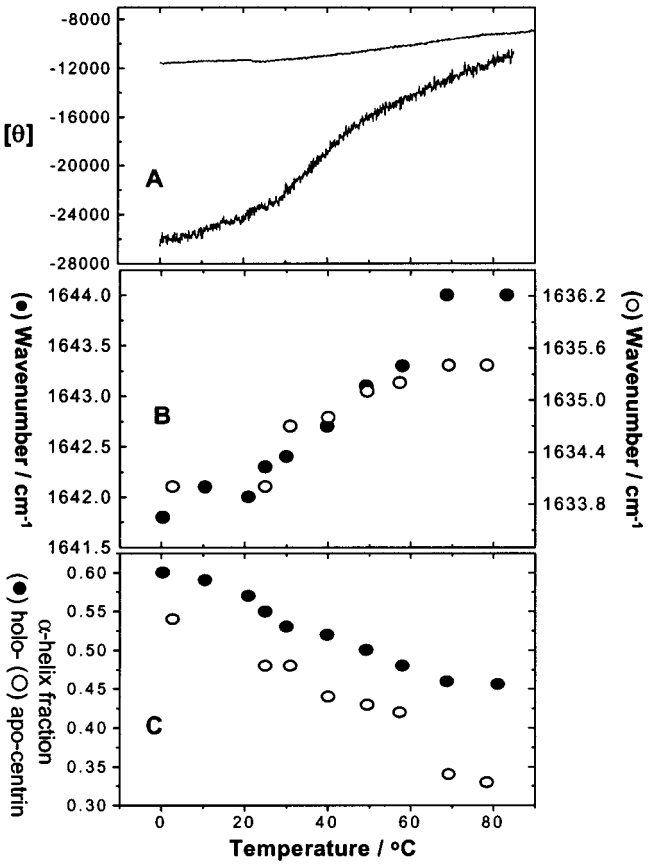

FIGURE 8: *Chlamydomonas* centrin temperature dependence plots for CD at λ 220 nm and FT-IR spectroscopies (A) of holocentrin, CD (thick, solid line), and apocentrin, CD (thin, solid line). (B) FT-IR α-helix frequencies for holocentrin (solid circles) in the spectral range of 1641.5−1644 cm^{-1} and for apocentrin (open circles) in the spectral range of 1633.4−1636.4 cm^{-1}. (C) Fraction of α-helix contribution as a function of temperature for (solid circles) holocentrin and (open circles) apocentrin based on the FT-IR curve-fitted spectral data.

DISCUSSION

To clarify features of centrin secondary structures and to resolve earlier discrepancies reported in the literature, we produced highly purified (99%) preparations of recombinant *Chlamydomonas* centrin.

We carried out FT-IR and CD spectroscopic studies of centrin in the presence and absence of cations. The results presented in Figure 3 of the overlaid FT-IR spectra of holocentrin and apocentrin summarize this paper very well. This novel approach toward the study of protein conformational changes has proven to be useful. Spectral changes that relate to the protein structure at the local level (aspartate) and its overall conformation (backbone) were observed. FT-IR spectral features were analyzed by a method first developed by Noda (*13*, *20*), known as 2D-FT-IR correlation. The generation of two-dimensional plots to resolve complex bands (such as amide I′ and side chain) was used to determine the position and number of subbands needed for curve fitting the FT-IR spectral data. More importantly, the combination of 2D-FT-IR and curve fitting allowed for a quantitative analysis of percent secondary structure and the determination of the normalized fraction of α-helical content for each form of the protein (apocentrin and holocentrin). In addition, 2D-FT-IR rendered a time line of events (structural changes) during thermal perturbation.

The aspartate and amide I′ modes were chosen to demonstrate the relationship between side-chain (local) and overall conformation (backbone) in centrin during thermal perturbation. Lysine absorbance was not considered due to its low molar extinction coefficient when compared to arginine. In the presence of cations the aspartate is coordinated (*26*, *27*) in a monodentate fashion (COO^-, 1568 cm^{-1}), affecting its carboxyl transition dipole moment and effectively lowering its vibrational energy level, as compared to the aspartate in its uncoordinated state (1578 cm^{-1}) according to Venyaminov's published work (*26*). Similar results have been reported for FT-IR studies of other calcium-binding proteins (*36*−*38*). The glutamate modes seem to also be affected by coordination with the cations or by salt bridging with arginine or lysine residues also reported in the study of a model helical peptide (*15*). Further investigation will be done in future studies by our laboratory using simulated 2D-FT-IR and molecular modeling. We will also investigate other overtones associated with the carboxylate vibrational modes.

CD was used to corroborate the overall change in centrin conformation and its behavior during the thermal perturbation in the presence and absence of cations. The CD spectral

analysis agrees with the FT-IR spectroscopic results for holocentrin and to a lesser degree with apocentrin reported herein. The differences could be due to the data set available for the CD analysis which did not account for a larger representation of calcium-binding proteins. A second possibility is the helix−helix interactions that have been observed to occur in other EF-hand proteins as a function of calcium (*39*, *40*). In addition, the estimated number of helical and β-strand segments also agrees with EF-hand calcium-binding proteins. The conformational transition observed for *Chlamydomonas* centrin was low at 45 and 37 °C within the temperature range studied (0−90 °C) in the presence and absence of cations but was also observed in CAVP (*41*) for the amino-terminal domain of this protein. This result does not preclude any other transition temperature, for the EF-hand family of proteins often have high thermal denaturation temperatures >90 °C. Thus, future studies involving differential scanning calorimetry will be carried out to verify the existence of these thermal denaturation transition temperatures for centrin in the absence and presence of cations. In general, the CD experiments revealed a conformational transition that involved mainly the α-helical to β-strand maintaining the random coil percent contribution of this protein constant. While the FT-IR analysis suggested similar trends for holocentrin, yet for apocentrin the conformational transition involved α-helical to β-strand and random coil changes.

We also intend for the future an in-depth study using sedimentation analysis, quasi-elastic light scattering, and calcium and magnesium titration experiments to further understand the calcium−magnesium antagonism reported earlier by Milos et al. (*42*) for EF-hand calcium-binding proteins. In this manner we will establish a paradigm of self-association for this protein. In addition, we will carry out DSC experiments for terminal peptides and the full-length protein in the presence and absence of cations to determine the thermal denaturation transition temperatures for *Chlamydomonas* centrin.

Our results agree with the reported NMR studies on *Chlamydomonas* centrin by Weber et al. (*9*), in that protein undergoes conformational change upon calcium binding. The differences in the results reported by Wiech (*10*) and Huang's group (*9*) may reside in the isolation and purification protocol followed by each group. We have taken care to use highly purified centrin (>99%) and to ensure its integrity as an apoprotein since calcium is a ubiquitous cation and care must be taken not to "contaminate" the protein. Our results suggest that these cations stabilize the protein during thermal perturbation, increasing its transition temperature by ∼8 °C when compared with its apo form.

Chlamydomonas centrin is a protein involved in the calcium-mediated contraction of fibers comprised almost exclusively of centrin. This calcium-binding protein has been found in the nucleous−basal body connectors, distal striated fibers, the stellate fiber, the basal bodies, and along the flagella. Thus, it is important to understand at the molecular level the conformational changes involved during cation binding and the determination of the relative stability of this protein in the presence and absence of cations. The differences in conformation of centrin (holo- and apo-forms) and the contraction of the fibers comprised primarily of centrin suggest a direct correlation between the protein conformation and the relaxation state of these fibers and flagella.

ACKNOWLEDGMENT

We thank Dr. Frank Prendergast for the use of the CD spectrophotometer in his laboratory and for helpful discussion on protein concentration determination. Dr. Pastrana thanks Dr. Cynthia McMurray for helpful discussions on protein self-association and also thanks Dr. Michel Pézolet and Dr. Henry Mantsch for discussions on two-dimensional FT-IR correlation analysis. We thank Dr. Dave Braddock for help in the design of the thermostated cell holder and shuttle. Dr. Pastrana thanks Susan Martinez for repeating some of the CD experiments. We thank Mike Holmes for the TOF mass spectrometry and Benjamin Madden for the partial amino acid sequencing of centrin at the Protein Core facility at Mayo Clinic and Foundation.

REFERENCES

1. Huang, B., Mengersen, A., and Lee, V. D. (1988) *J. Cell Biol. 107*, 133−140.
2. Moncrief, N., Kretsinger, R., and Goodman, M. (1990) *J. Mol. Evol. 30*, 522−562.
3. Salisbury, J. L., and Floyd, G. (1978) *Science 202*, 975−977.
4. Salisbury, J. L., Baron, A., Surek, B., and Melkonian, M. (1984) *J. Cell Biol. 99*, 962−970.
5. Salisbury, J. L. (1995) *Curr. Biol. 7*, 39−45.
6. Sanders, M. A., and Salisbury, J. L. (1989) *J. Cell Biol. 108*, 1751−1760.
7. Baron, A. T., Suman, V. J., Nemeth, E., and Salisbury, J. L.-(1994) *J. Cell Sci. 107*, 2993−3003.
8. Salisbury, J. L. (1998) *J. Eukaryotic Microbiol. 45*, 28−32.
9. Weber, C., Lee, V. D., Chazin, W. J., and Huang, B. (1994) *J. Biol. Chem. 269*, 15795−15802.
10. Wiech, H., Geier, M. B., Paschke, T., Spang, A., Grein, K., Steinkotter, J., Melkonian, M., and Schiebel, E. (1996) *J. Biol. Chem. 271*, 22453−22461.
11. Arrondo, J. L. R., Young, N. M. and Mantsch, H. H. (1988) *Biochim. Biophys. Acta 952*, 261−268.
12. Bandekar, J. (1992) *Biochim. Biophys. Acta 1120*, 123−143.
13. Noda, I. (1989) *J. Am. Chem. Soc. 111*, 8116−8181.
14. Graff, D. K., Pastrana-Rios, B., Venyaminov, S. Yu, and Prendergast, F. G. (1997) *J. Am. Chem. Soc. 119*, 11282−11294.
15. Pastrana-Rios, B. (2001) *Biochemistry 40*, 9074−9081.
16. Dalmas, B., and Bannister, W. H. (1995) *Anal. Biochem. 225*, 39−48.
17. Venyaminov, S. Y., and Yang, J. T. (1996) in *Circular dichroism and the conformational analysis of biomolecules* (Fasman, G. D., Ed.) pp 69−107, Plenum Press, New York.
18. Baron, A. T., Errabulo, R., Dinusson, J., and Salisbury, J. L. (1995) *Methods Cell Biol. 47*, 341−351.
19. Noda, I., and Ozaki, Y. (2000) *Appl. Spectrosc. 54*, 236A−248A.
20. Noda, I. (1990) *Appl. Spectrosc. 44*, 550−555.
21. Noda, I., Dowrey, A. E., and Marcott, C. (1993) *Appl. Spectrosc. 47*, 1317−1328.
22. Noda, I., Liu, Y., and Ozaki, Y. (1996) *J. Phys. Chem. 100*, 8665−8673.
23. Kawasaki, H., and Kretsinger, R. H. (1994) *Protein Profile 1*, 343−517.
24. Nakayama, S., Moncrief, N. D., and Kretsinger, R. H. (1992) *J. Mol. Evol. 34*, 416−448.
25. Kretsinger, R. H. (1987) *Cold Spring Harbor Symp. Quant. Biol. 52*, 499−510.
26. Venyaminov, S. Y., and Kalnin, N. N. (1990) *Biopolymers 30*, 1243−1257.
27. Chirdgaze, Yu. N., Fedorov, O. V., and Trushina, N. P. (1975) *Biopolymers 14*, 679−695.

28. Casal, H. L., Kohler, U., and Mantsch, H. H. (1988) *Biochim. Biophys. Acta 957*, 11−20.
29. Greenfield, N., and Fasman, G. D. (1969) *Biochemistry 8*, 4108−4116.
30. Sreerama, N., and Woody, R. W. (1993) *Anal. Biochem. 209*, 32−44.
31. Sreerama, N., and Woody, R. W. (1994) *Biochemistry 33*, 10022−25.
32. Sreerama, N. (1999) *Protein Sci. 8*, 370−380.
33. Johnson, W. C., Jr. (1999) *Proteins: Struct., Funct., Genet. 35*, 307−312.
34. Forsythe, G. E., Malcolm, M. A., and Moler, C. B. (1977) in *Computer Methods for Mathematical Computations*, Prentice-Hall, Englewood Cliffs, NJ.
35. van Stokkum, I. H. M., Spoelder, H. J. W., Bloemendal, M., van Grondelle, R., and Groen, F. C. A. (1990) *Anal. Biochem. 191*, 110−118.
36. Strynadka, N. C. J., and James, M. N. G. (1989) *Annu. Rev. Biochem. 58*, 951−998.
37. Masayuki, N., Mitsuo, T., Masaru, T., Toshifumi, H., Michio, Y., and Akihiro, T. (1994) *FEBS Lett. 349*, 84−88.
38. Mineyuki, M., Masayuki, N., Yue, K., Keiichi, K., Toshifumi, H., and Katsutoshi, N. (1997) *Eur. J. Biochem. 250*, 72−76.
39. El-Saleh, S., Warber, K. D., and Potter, J. D. (1986) *J. Muscle Res. Cell Motil. 7*, 387−404.
40. Herzberg, O., Moult, J., and James, M. N. G. (1986) *J. Biol. Chem. 261*, 2638−2644.
41. Baladi, S., Tsvetkov, P. O., Petrova, T. V., Takagi, T., Sakamoto, H., Lobachov, V. M., Makarov, A. A., and Cox, J. A. (2001) *Protein Sci. 10*, 771−778.
42. Milos, M., Schaer, J.-J., Comte, M., and Cox, J. A. (1986) *Biochemistry 25*, 6279−6287.

BI0157971